JACS
JOURNAL OF THE AMERICAN CHEMICAL SOCIETY

Article

pubs.acs.org/JACS

Microscopic Rates of Peptide–Phospholipid Bilayer Interactions from Single-Molecule Residence Times

Grant A. Myers,[†] Daniel A. Gacek,[†] Eric M. Peterson,[†] Christopher B. Fox,[†,‡,§] and Joel M. Harris*[,†,‡]

[†]Department of Chemistry, University of Utah, 315 South 1400 East, Salt Lake City, Utah 84112-0850, United States

[‡]Department of Bioengineering, University of Utah, 50 South Central Campus Drive, Salt Lake City, Utah 84112-9202, United States

Supporting Information

ABSTRACT: The binding of glucagon-like peptide-1 (GLP-1) to a planar phospholipid bilayer is measured using single-molecule total internal reflection fluorescence microscopy. From several reports in the literature, GLP-1 has been shown to be a random coil in free solution, adopting a folded, α-helix conformation when intercalated into membrane environments. Single-molecule fluorescence measurements of GLP-1 binding to supported lipid bilayers show evidence of two populations of membrane-associated molecules having different residence times, suggesting weakly adsorbed peptides and strongly bound peptides in the lipid bilayer. The path to and from a strongly bound (folded, intercalated) state would likely include an adsorbed state as an intermediate, so that the resulting kinetics would correspond to a consecutive first-order reversible three-state model. In this work, the relationships between measured single-molecule residence times and the microscopic rates in a three-state kinetic model are derived and used to interpret the binding of GLP-1 to a supported lipid bilayer. The system of differential equations associated with the proposed consecutive-three state kinetics scheme is solved, and the solution is applied to interpret histograms of single-molecule, GLP-1 residence times in terms of the microscopic rates in the sequential two-step model. These microscopic rates are used to estimate the free energy barrier to adsorption, the fraction of peptides adsorbing to the membrane surface that successfully intercalate in the bilayer, the lifetime of inserted peptides in the membrane, and the free energy change of insertion into the lipid bilayer from the adsorbed state. The transition from a random coil in solution to a folded state in a membrane has been recognized as a common motif for insertion of membrane active peptides. Therefore, the relationships developed here could have wide application to the kinetic analysis of peptide–membrane interactions.

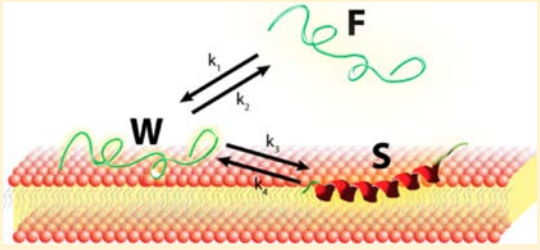

1. INTRODUCTION

The membrane catalysis hypothesis[1−3] suggests that signaling peptides targeting membrane-resident receptors must first interact with the membrane bilayer before binding with their receptor. According to this model, membrane interactions can facilitate ligand–receptor binding in several ways. First, interactions of the peptide with the membrane effectively concentrate the ligand near the receptor. Second, the reduced dimensionality of diffusion across the membrane to the receptor can be more efficient than three-dimensional diffusion through solution. Finally, conformational changes associated with membrane binding can effectively pre-fold the peptide structure and position it within the membrane for receptor binding. Thus, interactions between signaling peptides and cell membranes can play a critical role in membrane-resident receptor binding. In this work, we analyze single-molecule fluorescence imaging data to extract the microscopic rates of peptide–membrane association, applying this method to the study of glucagon-like peptide-1 (GLP-1) and its interactions with a supported lipid bilayer.

GLP-1 is an incretin, a 30-residue peptide hormone of the digestive system that has been linked to systemic insulin and glucagon levels.[4] Because of their effects on blood glucose levels, synthetic analogues of GLP-1 have been successfully developed as treatments for type-2 diabetes.[5] The target of this hormone is a G protein-coupled receptor, located in cell membranes throughout the body including pancreas, lung, gastrointestinal tract, and central nervous system.[6] Like many membrane-active peptides,[3,7] GLP-1 undergoes a significant conformational change upon binding to a phospholipid membrane. The peptide exists as a random coil in solution but folds into an α-helix in the amphipathic environment of the cell membrane.[8−11] Recently, X-ray crystallography has shown that GLP-1 is indeed in an α-helix conformation when bound to its receptor.[12]

It is expected that the transition of GLP-1 from a random-coil peptide in solution to a folded state in a membrane should involve a significant release of enthalpy, to compensate for the entropy penalty of a folded peptide.[7] This step should represent a kinetic barrier, where the peptide may arrive, adsorb, and leave the membrane before transitioning to a more stable, folded state. Membrane binding studies of other amphipathic peptides[13,14] have reported evidence of two membrane dissociation rates. In preliminary work from this laboratory,[15] evidence of two populations of GLP-1, weakly and strongly

Received: June 21, 2012
Published: November 14, 2012

associated with a supported lipid bilayer, was found in the residence times of individual fluorescently labeled GLP-1 molecules, determined from images acquired by total internal reflection fluorescence (TIRF) microscopy. The observed residence time histograms were biexponential, suggesting two rates for peptides leaving the membrane.[15] In this previous work, the relationships between the measured rates and elementary kinetic steps of peptide−membrane interactions were not developed. In the present work, a kinetic model is proposed that would account for the observed single-molecule residence times in terms of the microscopic rates of peptide association and intercalation in the membrane. This model is applied to new measurements of the number density and residence times of fluorescently labeled GLP-1 interacting with a 1,2-dipalmitoyl-*sn*-glycero-3-phosphocholine (DPPC) planar lipid bilayer supported on glass, where microscopic rate constants of peptide−membrane association are determined from a fit of the three-state kinetic model to the results.

2. THEORY

2.1. Three-State Model of Membrane Association. If the insertion of a folded peptide into a lipid membrane involves a reversible adsorption step at the membrane−solution interface, the resulting kinetics can be described by a consecutive two-step, three-state scheme, illustrated in Figure 1. This model assumes that the free solution peptide, F, cannot access the strongly associated folded state, S, directly from solution without first residing at the interface in state W. The principle of microscopic reversibility,[16−18] which has been demonstrated in studies of protein folding at equilibrium,[19] holds that the transition state for a reversible reaction is the same regardless of the direction of the reaction. Based on this principle, if the weakly bound state is an intermediate to peptide folding and strong binding, then this weak state will also be in the path from the strongly bound state to free solution at equilibrium.

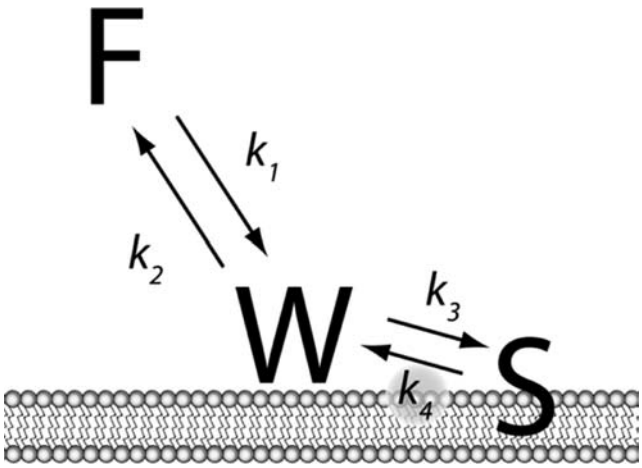

Figure 1. Proposed three-state kinetic model for the interaction of a membrane-active peptide with a phospholipid bilayer, where a free peptide in solution, F, adsorbs to the bilayer in a weakly bound state, W, followed by folding and insertion into the bilayer in a strongly associated state, S.

In this model, the constants, k_1 through k_4, represent the rate constants for the transitions between these three populations. The heterogeneous rate constant k_1 describes the rate of molecules adsorbing to the membrane from solution. The rate constant k_2 characterizes the rate of desorption of weakly associated peptide from the membrane surface. The rate constant k_3 is the intercalation rate, where molecules transition from the weakly associated, adsorbed state to the longer-lived folded and membrane-inserted state. The rate constant k_4 describes a process where molecules reemerge from the folded state to the weakly bound surface-adsorbed state, at which point the molecules may either leave the surface (at a rate k_2), or return to the strongly associated state (at a rate k_3).

When residence times of individual labeled GLP-1 peptides are measured using TIRF microscopy, the cumulative residence time histogram is well described by a biexponential decay[15] (see results below):

$$H(t) = P_1\, e^{-t/\tau_1} + P_2\, e^{-t/\tau_2} \quad (1)$$

where the observed time constants are inversely related to the decay rates of the two apparent populations, $r_1 = 1/\tau_1$ and $r_2 = 1/\tau_2$, and the pre-exponential coefficients P_1 and P_2 represent the relative numbers of events from these two populations. Note that the histograms in the present work are integrated or cumulative residence times, which report the number of molecules that survive for the time on the *x*-axis, and the *y*-axis intercept is the total number of molecules; it has been shown that cumulative histograms are much more sensitive to heterogeneity in kinetic populations.[20] It is tempting to conclude that the longer residence time corresponds to the lifetime of the folded peptide, S, in the membrane and the shorter residence time represents desorption of W from the membrane surface. This interpretation ignores the fact that the kinetic steps are strongly coupled. For example, the emergence of a folded peptide to the membrane surface does not immediately lead to its desorption into solution; both desorption (k_2) and reinsertion (k_3) extend the lifetime of the peptide on or within the membrane upon its reemergence to the membrane surface. The goal of this section, therefore, is to derive the relationship between the measured single-molecule residence times and pre-exponential factors in eq 1 and the microscopic rate constants described by the kinetic model in Figure 1; this relationship can then be used to interpret membrane association kinetics of GLP-1 or other membrane-active peptides.

2.2. Interpreting Single-Molecule Residence Time Histograms. The relationships between the measured parameters from residence time histograms and the intrinsic microscopic rate constants are determined by an analysis of the system of differential equations associated with the three-state reversible first-order system illustrated in Figure 1.

$$\frac{\partial F}{\partial t} = -k_1 F(t)\lambda^{-1} + k_2 W(t)\lambda^{-1}$$
$$\frac{\partial W}{\partial t} = k_1 F(t) - (k_2 + k_3)W(t) + k_4 S(t)$$
$$\frac{\partial S}{\partial t} = k_3 W(t) - k_4 S(t) \quad (2)$$

where F, W, and S are the concentrations of the respective populations and λ^{-1} is the ratio of the surface area of the bilayer to the volume of the solution that accounts for the change in dimensionality. This system of equations is one of a few multistep kinetic schemes having an analytical solution. While the general solutions are cumbersome (see Supporting Information), particular solutions to the system have been

dx.doi.org/10.1021/ja306074k | J. Am. Chem. Soc. 2012, 134, 19652−19660

published as early as the turn of the last century.[21−23] For the present application, symbolic computational methods were used to solve the general system of differential equations explicitly and then to apply boundary conditions to the results to obtain the analytical relationships between the individual rate constants of adsorption, intercalation, emergence, and desorption from the parameters determined from single-molecule residence histogram measurements.

The information contained in a histogram of residence times is derived from the random arrival of molecules at the membrane surface; these molecules associate with the membrane for a period of time and then leave. To construct a histogram of residence times, all of the events measured during an experiment are aligned onto a new time axis, so that each event begins at time zero (see Figure 2). This realignment

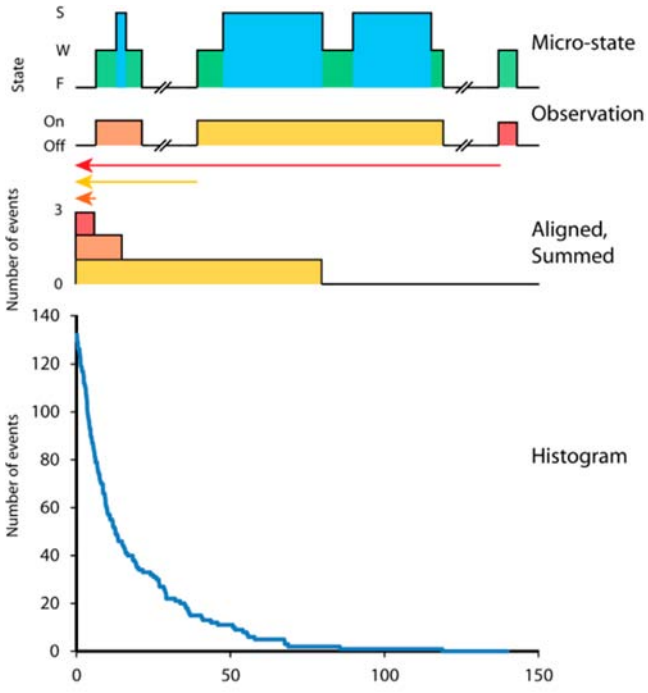

Figure 2. Construction of a single-molecule cumulative residence time histogram. Top trace shows the binding state of three molecules arriving and leaving the lipid bilayer; peptides arrive at the bilayer surface in the weakly bound state and may transition into the folded, strongly bound state. The observation of a molecule in a fluorescence image cannot distinguish between microstates of the bound peptide. To construct a histogram, all observed events are aligned onto a new time axis having an origin that coincides with the arrival of each molecule; these events are then summed on this new axis to produce a cumulative residence time histogram.

of the data establishes the first of two boundary conditions for solving the differential equations. First, because all of the molecules arrive at time $t = 0$ on the membrane surface, then within the assumptions of the three-state model, they all begin in the weakly bound or adsorbed state, so that the initial condition for the normalized population is $W(t = 0) = 1$ and $S(t = 0) = 0$. Some of the adsorbed molecules may then leave the surface without transitioning to the strongly bound state, while other molecules may successfully transition between the weakly and strongly bound states, and thus persist for a longer time before leaving the surface (see Figure 2). A second constraint arises from the very low surface density of peptides observed in these experiments, where the probability of an interrogated spot being doubly occupied is very small, less than 1.2% (see below). As a result, kinetics reported in the residence time histograms have no significant contribution from an additional molecule binding to the membrane surface within an interrogated spot, prior to the original molecule leaving; therefore, the adsorption rate is neglected in the kinetic analysis, $k_1 = 0$.

When these two constraints are applied to the system of differential equations (see Supporting Information), the time dependences of the two surface populations, $W(t)$ and $S(t)$, are *both* biexponential functions, having different pre-exponential factors but sharing the same pair of rates:

$$r_1 = \frac{1}{2}(k_2 + k_3 + k_4 + \sqrt{(k_2 + k_3 + k_4)^2 - 4k_2k_4}) \tag{3a}$$

$$r_2 = \frac{1}{2}(k_2 + k_3 + k_4 - \sqrt{(k_2 + k_3 + k_4)^2 - 4k_2k_4}) \tag{3b}$$

These functions are summed to obtain the time dependence of the entire surface population, $H(t) = W(t) + S(t)$. The result is biexponential decay without offset, corresponding exactly to the form of eq 1, $H(t) = P_1\, e^{-tr_1} + P_2\, e^{-tr_2}$, where r_1 and r_2 are given by eqs 3a and 3b, while P_1 and P_2 are given by

$$P_1 = \frac{k_2 - k_3 - k_4 + (r_1 - r_2)}{2(r_1 - r_2)} \tag{4a}$$

$$P_2 = \frac{-k_2 + k_3 + k_4 + (r_1 - r_2)}{2(r_1 - r_2)} \tag{4b}$$

While these expressions predict the observed rates and pre-exponential factors for single-molecule residence time histograms from the intrinsic reaction rates, k_2, k_3, and k_4, they can be readily rearranged so that the intrinsic rates can be determined from measured residence time histograms. The resulting relationships derived for determining the intrinsic rates from measurable quantities are remarkably simple. For example, the rate constant for molecules leaving the surface, k_2, is the population-weighted average of the two observed rates in the histogram decay:

$$k_2 = \frac{P_1r_1 + P_2r_2}{P_1 + P_2} \tag{5}$$

The rate constant for molecules transitioning from the strongly associated state back to the weakly associated, adsorbed state is the ratio of the product of the histogram rates to the intrinsic rate constant for molecules leaving the surface:

$$k_4 = \frac{r_1r_2}{k_2} \tag{6}$$

Finally, the rate constant of molecules transitioning from the weakly associated to the strongly associated state is given by the difference between the sums of the histogram decay rates and the intrinsic reverse rate constants:

$$k_3 = (r_1 + r_2) - (k_2 + k_4) \tag{7}$$

These expressions will be used in this work to interpret histograms of GLP-1 residence times in supported lipid bilayers, but they are useful generally for interpreting two-

dx.doi.org/10.1021/ja306074k | J. Am. Chem. Soc. 2012, 134, 19652−19660

state binding kinetics from single-molecule imaging experiments.

2.3. Interpreting Single-Molecule Binding Isotherms. The general solution to the system of differential equations for the three-state model of membrane association can also be used to interpret the equilibrium population of molecules at the membrane surface. These data are generally collected as an isotherm, where the number densities of membrane-associated molecules are measured by counting fluorescent spots in a known area as a function of solution concentration.[15] Because the fluorescence image data cannot distinguish whether molecules are weakly or strongly bound, the measured isotherm reports the total equilibrium population density, $W_{eq} + S_{eq}$. The ratio of this total surface concentration and the free solution concentration, F_{eq}, is the slope of the isotherm and the equilibrium constant for binding, K_0. This ratio can be derived from the general solution to the system of eq 2, under the assumption that the initial (arbitrary) populations, $F(0)$, $W(0)$, and $S(0)$, have evolved over long times ($t \gg 1/r_2$) to their equilibrium values (see Supporting Information):

$$\frac{W_{eq} + S_{eq}}{F_{eq}} = K_0 = \frac{k_1k_4 + k_1k_3}{k_2k_4} \tag{8}$$

It is useful to note that k_0 is a ratio of a surface concentration (molecules/area) to a solution concentration (molecules/volume), and thus has units of distance. This distance is meaningful and represents the depth into solution above the surface that contains the same number of molecules that are bound to a given surface area.[24,25]

This expression can be easily rearranged to solve for the rate constant k_1, which characterizes adsorption of peptides to the membrane from solution:

$$k_1 = K_0\frac{k_2k_4}{k_3 + k_4} \tag{9}$$

Note that k_1 is a heterogeneous rate constant having units of velocity (cm s^{-1}) and characterizes the rate of collision and adsorption of molecules from solution to the membrane surface. It is analogous to the use of heterogeneous reaction rates in electrochemistry,[26] which describe the rates of collision and electron transfer with an electrode surface. Finally, eq 9 shows that by combining information from the slope of the binding isotherm, K_0, with rate constants, k_2, k_3, and k_4, from the analysis of histograms of single-molecule residence times, one can determine all four rate constants in the three-state kinetic model.

Note that as the rate constant for peptide folding and membrane insertion, k_3, goes to zero, the kinetic model reverts to a simple two-state system, and eq 8 simplifies to $K_0 = k_1/k_2$, which describes a simple adsorption equilibrium. Setting k_3 equal to zero in eq 3, shows that the histogram of single-molecule residence times becomes single exponential, where $r_1 = k_2$ and r_2 = zero, so that the desorption rate of the simple two-state system is k_2. In the three-state system, the effective desorption rate, $[k_2\ k_4/(k_3 + k_4)]$ (see eq 9), becomes proportionally slower. The factor slowing the off-rate relative to k_2 is $[k_4/(k_3 + k_4)]$, and this factor represents the fraction of membrane-associated peptides that are weakly bound. When k_3 is large compared to k_4, most of membrane-bound peptides are folded and inserted, and the effective rate of molecules leaving the membrane is reduced by the small fraction of peptides in the W state that can leave the membrane surface.

3. MATERIALS AND METHODS

3.1. Sample Preparation. To characterize the interactions of GLP-1 with a phospholipid bilayer, fluorescently modified glucagon-like peptide was synthesized using solid-phase peptide synthesis. A Cy3B fluorescent maleimide label (GE Amersham) was covalently attached to a cysteine bound via a 20-atom polyethylene-glycol water-soluble linker (Novabiochem) to the C-terminus of the 30-residue peptide.[15] The sequence of labeled GLP-1 is HAEGTFTSDVSSY-LEGQAAKEFIAWLVKGR-PEG_2-cysteine-Cy3B (maleimide). The labeled peptide was purified by reverse-phase chromatography and its molecular weight verified by matrix-assisted laser desorption-ionization mass spectrometry (see Supporting Information). Dipalmitoyl-phosphatidylcholine (DPPC) phospholipid bilayers were deposited onto the microscope coverslips using a Langmuir−Blodgett/Langmuir−Schaeffer technique.[27,28] Glass coverslips were cleaned in a piranha solution, 60:40 concentrated H_2SO_4: 30%H_2O_2, then rinsed and stored in ultrapure (Barnstead) water; caution: piranha is a corrosive solution that can cause skin or eye burns and can react explosively with organic compounds. After filling the Langmuir trough (KSV Instruments) with ultrapure water, a clean coverslip was immersed in the water subphase and 47 μL of 1 mg/mL DPPC in chloroform was deposited on the air−water interface. Following evaporation of the chloroform, the barriers were closed, compressing the lipid monolayer to a surface pressure of 35 mN/m or ~53 $Å^2$/molecule, and the coverslip was raised through the subphase surface at a rate of 4 or 5 mm/min to deposit a lipid monolayer. The coverslip was then positioned parallel to the trough surface, after which it was pushed down quickly through the lipid film (~40 mm/min) to form a bilayer. The transfer ratios for the upward and downward depositions were ~1 and ~1.2, respectively. The slightly larger transfer ratio for the second layer may be due to some lipid sticking to the backside of the coverslip dipping apparatus.[29] The flow cell with coverslip-supported lipid bilayer was assembled under water so that the bilayer was not exposed to an air−water interface. Fluorescence images of deposited DPPC lipid bilayers by Nile red staining show a uniform intensity distribution and no resolvable defects.

3.2. Instrument Description and Experimental Protocols. Through-the-objective TIRF microscopy[30] was used to selectively excite individual fluorescent peptide molecules at the glass/water interface. The microscope system consisted of a diode laser (B&W Tek) at 532 nm fiber-coupled into an Olympus IX71 microscope with 60x, TIRF objective having numerical aperture, NA = 1.45. Images of single molecules were collected at a framing rate of 10 Hz using an electron-multiplying charge coupled-device (CCD) camera (Andor $iXon^{EM}$+ 897).

To determine the equilibrium constant for binding, isotherm experiments were performed in which the number densities of peptides in the bilayer were measured with three or more replicates for each of several peptide concentrations ranging from 4 pM up to 100 pM with acquisitions of 100 or more frames. To measure single-molecule residence time histograms, 50 pM peptide solutions were equilibrated with a fresh bilayer in the microscope cell and images were acquired using a laser power of 3 mW in the collimated beam at the rear of the microscope, corresponding to an excitation power density of 24 Wcm^{-2} at the sample surface. The total acquisition times were 300 s (3000 frames), again with three replicates. To characterize the effects of laser power on measured histogram parameters for Cy3B-labeled peptide excited at 532 nm, identical experiments were performed with two replicates each at laser powers ranging from 1.8 to 11.1 mW in the collimated beam at the rear of the microscope. Experiments were carried out at room temperature, ~22 °C.

3.3. Image Analysis. The number densities of peptide molecules bound to the lipid bilayer and their residence times were extracted from fluorescence images using an adjacent-pixel criterion[31] to identify the locations of molecules in each frame. The signature of a fluorescent spot from a molecule is distinguished from the random (single-pixel) fluctuations in the background by requiring that the intensity occupy an area on the camera face comparable to the diffraction-limited point spread function, which has a $1/e^2$ diameter of 2.4 pixels or 0.64 μm in

dx.doi.org/10.1021/ja306074k | J. Am. Chem. Soc. 2012, 134, 19652−19660

the sample plane. This criterion is enforced by requiring that both the intensity of a central bright pixel and at least one of the eight pixels adjacent to the bright pixel exceeds a threshold of 3.0-times the standard deviation of the background. While the probability of a single pixel from the background exceeding this threshold is significant, 4.9×10^{-4} or 32 pixels per 256-by-256 pixel frame, the probability that one of the 8 pixels adjacent to any of these 32 pixels will also exceed the threshold is quite small, $8*32*4.9 \times 10^{-4}$ or 0.125 false spots per frame or one event in every eight frames.

To determine residence times of each peptide in the lipid bilayer, the locations of all molecules in each frame of the acquisition were recorded and then analyzed using an algorithm which can extend the measured residence times over photoblinking events[32−36] of the single dye label. For every identified molecule in a frame, 10 subsequent frames were searched for molecules centered at the same pixel position or in one of the surrounding 8-pixels on the perimeter of the original central pixel to allow for the uncertainty in the measurement of molecular positions in a given frame. Note that for the gel-phase lipids used in this study, the diffusion of molecules across the surface was not detectable on the time scales of the experiment, greatly simplifying the analysis of molecular residence times. If subsequent frames indicate a molecule in the region in question, the residence time for that molecular event was incremented by the appropriate amount. Then, starting with the last frame in which the molecule was identified, the 10-forward-frame search was repeated until the entire residence time of the molecule was determined. Using this method, photoblinking events or random fluctuations that caused the intensity to fall below the threshold for as many as 10 frames (1 s) were "bridged". The duration of the bridging search was optimized by examining the stability of the fitted kinetic parameters relative to the length of the bridge; a one-second bridge was found to produce consistent kinetic results for the longer-lived population of bound peptides (see Supporting Information). Molecules exhibiting residence times of only a single frame were dropped from the analysis to avoid counting events arising from peptides in solution briefly visiting the 150-nm evanescent wave region at the bilayer surface. For accumulation of data into a residence time histogram, molecular events that started in the first or last 10 frames of the acquisition were also neglected because of their unknown total residence times.

When bridging brief off-states of the dye label in order to report more accurate residence times, there is a chance that a new molecule from solution will bind to the membrane in the area previously identified as occupied and lead to an increase in the reported residence time. To calculate the probability of this occurring, we take the product of the heterogeneous binding rate constant, $k_1 \approx 1 \times 10^{-4}$ cm s^{-1} (see below), the area of a 9-pixel site projected back through the collection optics onto the sample surface (0.64 μm^2), and the solution concentration of peptide (50 pM = 3×10^{10} molecules/cm^3). The product of these factors is the binding rate from solution to the site area, 1.9×10^{-2} molecules $site^{-1}$ s^{-1} or ~52 s between such events. The time between binding events is thus 520 frames, or 52 times greater than the 10-frame bridge for a new molecule to arrive at a resolvable site when the peptide concentration is 50 pM. Thus, when using this algorithm, there is <2% probability that a recorded residence time will be extended by the arrival and binding of a new peptide from solution (see Supporting Information).

4. RESULTS

4.1. Binding of GLP-1 to DPPC Lipid Bilayers. To observe the population and residence times for GLP-1 on a lipid membrane, a DPPC bilayer was deposited onto a glass coverslip and exposed to varying concentrations of Cy3B-labeled GLP-1 in buffered solutions. Fluorescence images of the labeled peptide on the lipid bilayer were acquired, and from those images, molecular spots were identified and counted. The average intensity of labeled peptide fluorescence spots was 87 photoelectrons (PEs) for the brightest pixel and 66 PEs for the next brightest pixel, both of which are much greater than the 37-PE detection threshold (3.0 standard deviations above background) used to identify molecular spots. Intensity distributions of Cy3B-labeled GLP-1 fluorescence spots are plotted in Supporting Information and used to determine the probability of missing molecules in an image (false negatives). This probability was evaluated by fitting the distribution of measured intensities and determining what fraction of second brightest pixels fall below the detection threshold; from these results (see Supporting Information), the false-negative probability or fraction of GLP-1 molecules that are missed in a given image is small, less than 7%. An example fluorescence image with identified molecular spots is shown in Figure 3.

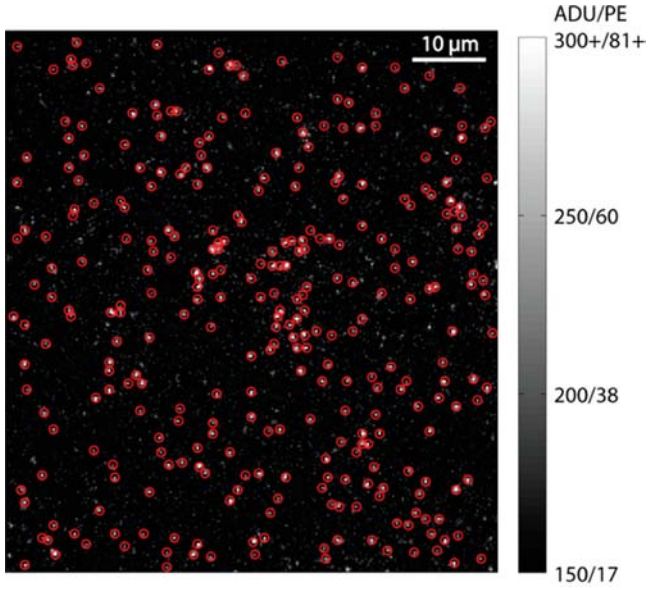

Figure 3. Fluorescence image (100 ms frame) of Cy3B-labeled GLP-1 associated with a DPPC supported lipid bilayer from a 50 pM solution of the peptide. The red circles indicate where molecular spots are identified based on the adjacent pixel criterion. Gray scale indicates both analog-to-digital units (ADU) and photoelectrons (PE).

To determine the equilibrium constant for GLP-1 binding to a DPPC bilayer, the number densities of molecules in the bilayer were measured by imaging and counting labeled-peptide spots versus solution concentration; the data from three replicates at each peptide concentration, which ranged from 4 pM up to 100 pM, are plotted in Figure 4. Two control experiments were performed to check the validity of these results. First, to test whether any defects in the lipid bilayer might lead to anomalous binding results, the adsorption affinity of the Cy3B-labeled peptide to a clean glass substrate was measured and found to be a small fraction (15%) of that observed on a DPPC bilayer (see Supporting Information). These data show that GLP-1 interacting with glass at any defects in the lipid bilayer would be weakly adsorbed. A second control was performed to determine whether the combined Cy3B and PEG tether used for labeling would contribute to the affinity of the GLP-1 peptide for the lipid bilayer. A model compound was synthesized containing Cy3B-maleimide labeled cysteine bound to the 20-atom polyethylene-glycol linker. As shown in Supporting Information, this compound exhibited negligible affinity for a DPPC bilayer, producing spot densities that were 0.01% of those observed for the labeled GLP-1 peptide at equivalent solution concentrations.

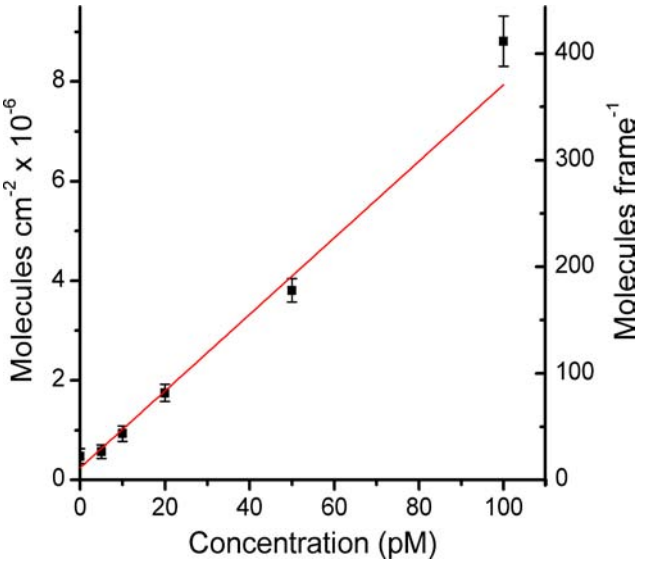

Figure 4. Isotherm plot of GLP-1 binding to a DPPC lipid bilayer. The average number of molecules in a 68 × 68 μm image (right axis) and the corresponding number density (left axis) are plotted versus solution concentration, together with a least-squares fitted straight line (red).

The relationship between the number density of GLP-1 molecules interacting with the lipid bilayer and their solution concentration is linear, as shown in Figure 4, with a small intercept from fluorescent spots in the blank images. The slope of the isotherm data, $\Gamma/C = 2.2(\pm0.1) \times 10^{17}$ cm^{-2} M^{-1} can be related to the equilibrium constant for GLP-1 binding to the lipid bilayer through a simple units conversion, K_o = 1000 cm^3 L^{-1}/CN_{Av} = 3.6(±0.2) × 10^{-4} cm or 3.6 μm. This result represents the distance into solution that contains the same number of molecules as reside at equilibrium in the lipid bilayer area below it.[24,25] This result not only characterizes the membrane-bound population and corresponding affinity of the peptide for the lipid bilayer at equilibrium, it is also needed to determine the rate of GLP-1 adsorption to the bilayer surface from solution (see below).

The linearity of the isotherm results in Figure 4 is consistent with a lack of spot overlap over this concentration range, which assures that the probability of any interrogated (9-pixel) region being doubly occupied is small. At a solution concentration of 50 pM GLP-1 used for residence time kinetic experiments (see below), the density of molecular spots is 175 per frame, and their corresponding 9-pixel regions occupy a small fraction (2.5%) of the total image area. Based on a Poisson statistical model for spatially resolving spots in the image,[31,37] the expected number of overlapped spots at this surface coverage is 2.1 out of 175, corresponding to a probability of a spot being doubly occupied of 1.2%. This result is critical to the kinetic model developed for the residence time histograms (see above); the lack of doubly occupied spots supports the assumption that there is a small probability of an additional molecule binding within an interrogated region before the original molecule leaves the membrane. This allows the adsorption rate, k_1, in the kinetic analysis of the residence times to be neglected.

4.2. Kinetics of GLP-1 Binding to DPPC Lipid Bilayers. The observation of labeled GLP-1 molecules bound to a lipid membrane provides not only a direct count of the membrane-associated peptide population but also the residence times of individual molecules, which allow the kinetics of their binding and unbinding to be determined. Residence times are determined by correlating the locations of detected fluorescent spots between frames, reporting the total length of time of a molecular visit. Single-frame events were neglected in the analysis, as were molecules present at the start or the end of the acquisition whose residence time is unknown.

From these data, a histogram of residence times is constructed where every event measured in an experiment is aligned on a common time axis, where each event begins at time zero (see Figure 2, above). In this cumulative histogram, all of the molecular events contribute to the total until the point in time when the molecule leaves the image. An example residence time histogram is plotted in Figure 5, which shows

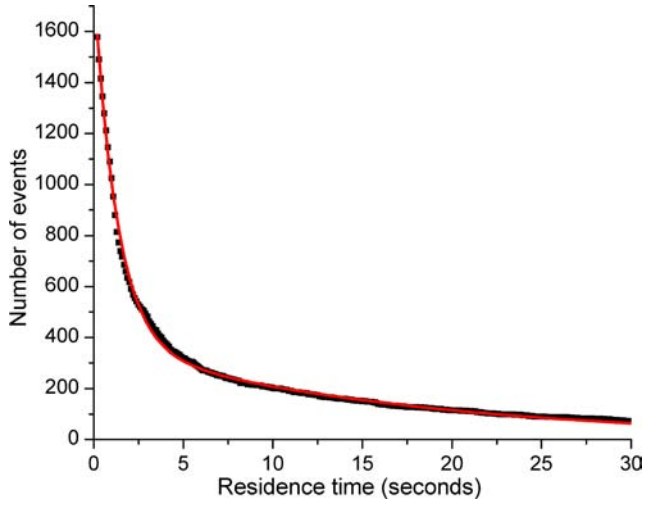

Figure 5. Example cumulative residence time histogram for GLP-1 binding to a DPPC supported lipid bilayer. Data points (black) are fit to a biexponential model, eq 1, with no offset (red line).

the biexponential decay of the probability of individual GLP-1 peptides leaving the lipid bilayer consistent with predictions of eqs 3a and 3b; a log–linear plot of these results is also including Supporting Information.

From three replicates of the residence time histogram experiment, the parameters from the fit of the data to the biexponential model, eq 1, averaged as follows: τ_1 = 1.19 ± 0.05 s, τ_2 = 19 ± 2 s, and the pre-exponential fraction, $P_1/(P_1 + P_2)$ = 0.83 ± 0.03, where the average number of molecular events measured in each of the three experiments was 1200 ± 300. The apparent residence time of a labeled peptide in the lipid bilayer can be shortened by photobleaching of the dye label. The influence of photobleaching on the kinetic results was tested by acquiring residence time data at several excitation laser powers. The results show that the measured time constants do not change within their uncertainties up to a laser power of 4.5 mW, above which the longer time constant decreases significantly (see Supporting Information). The reported isotherms and histograms were acquired with 3.0 mW excitation, well below the power level where photobleaching influences the measured residence times. Finally, the robustness of the kinetic parameters derived from residence time histograms was tested by acquiring on different days, using different microscope systems, and with Cy3 and Cy3B labeling

dx.doi.org/10.1021/ja306074k | J. Am. Chem. Soc. 2012, 134, 19652–19660

of the GLP-1 peptide. The results show remarkable consistency as shown in a tabulated comparison in Supporting Information.

The kinetic parameters, $P_1/(P_1+P_2)$, $r_1 = 1/\tau_1$ and $r_2 = 1/\tau_2$, from the residence histogram above were substituted into eqs 5−7 to determine the microscopic rate constants for GLP-1 peptide association with a DPPC lipid bilayer based on the proposed three-state reversible model. The rate constant for weakly associated peptides desorbing from the surface of the bilayer into solution was determined to be $k_2 = (7.0 \pm 0.2) \times 10^{-1}$ s^{-1}, which corresponds to a desorption lifetime of 1.43 ± 0.04 s. Desorption from the lipid bilayer surface competes with intercalation of surface-associated peptides, transitioning to a strongly bound, folded state in the membrane, which occurs at a 5.4-fold slower rate, $k_3 = (1.3 \pm 0.2) \times 10^{-1}$ s^{-1}. The ratio of this rate of intercalation to the sum of intercalation and desorption rates, $k_3/(k_2 + k_3)$, is the fraction of peptides that adsorb to the membrane surface that successfully fold and intercalate into the membrane before they desorb. From the present results, this fraction of arriving peptides that intercalate is relatively small, 0.17 ± 0.3.

The rate constant for molecules emerging from the strongly bound, intercalated state to the weakly associated, adsorbed state, k_4, $= (6.5 \pm 0.7) \times 10^{-2}$ s^{-1}, is an order of magnitude slower than rate of desorption of GLP-1 from the lipid bilayer surface, k_2. This result indicates that the intercalated population significantly lengthens the lifetime of GLP-1 in the membrane. Indeed, the majority of the GLP-1 peptide associated with the membrane at equilibrium is intercalated; this fraction is determined by the competition between intercalation of the adsorbed population and the rate of reemergence, where $k_3/(k_3 + k_4) = 0.67$, indicates the fraction of GLP-1 population that is strongly bound. From the ratio of rates of reemergence and intercalation, one may calculate the Gibbs free energy difference between intercalated and surface adsorbed states of the peptide, where $\Delta G = -RT \ln(k_3/k_4) = -1.7(\pm 0.3)$ kJ mol^{-1} at 298 K. This small free energy difference likely represents a balance between the energy costs of creating free volume within the lipid bilayer and the reduction of conformational freedom of the peptide with changes in the degree of water contact with hydrophobic residues of the peptide, as it transfers from membrane−solution interface to the membrane interior.

The final rate constant to be determined from the data is for the adsorption of the peptide to the lipid bilayer from solution. This rate is found by substituting the effective off-rate for GLP-1 dissociation from the lipid bilayer, $[k_2\, k_4/(k_3 + k_4)]$, and the binding equilibrium constant determined from the accumulation isotherm, K_o into eq 9. The resulting heterogeneous rate constant is $k_1 = (1.02 \pm 0.03) \times 10^{-4}$ cm s^{-1}. This rate constant can be compared with the frequency of collisions between molecules and the lipid bilayer to determine what fraction of the collisions lead to association of the peptide with the membrane. To predict the collision frequency, the diffusion coefficient of the peptide can be estimated by the Stokes−Einstein equation, where the peptide in solution is assumed to be a random coil[8−10] with a hydrodynamic radius, $r \approx 1.3$ nm.[38,39] From the Stokes−Einstein equation and the viscosity of water, the diffusion coefficient of the peptide at 298 K is estimated to be $D = k_B\, T/6\pi\eta r \approx 1.6 \times 10^{-6}$ cm^2 s^{-1}. The diffusion-controlled heterogeneous reaction velocity is predicted by Fick's first law[26] to be the flux through a unit area for a given solution concentration, $v = J/C = D(\mathrm{d}C/\mathrm{d}x)/C$, where the gradient, $(\mathrm{d}C/\mathrm{d}x)$, is the bulk solution concentration divided by the encounter distance for reaction,[40] estimated to be about twice the hydrodynamic radius of the peptide. The bulk solution concentration thus cancels, and the diffusion-limited reaction velocity is estimated to be $v = J/\mathrm{d}x \approx D/2r \approx 7$ cm s^{-1}. Dividing k_1 by the diffusion-limited rate provides an estimate of the fraction of collisions between the peptide and lipid bilayer surface that result in adsorption, $k_1/v \approx 1.5 \times 10^{-5}$. This result shows that adsorption of the GLP-1 peptide to the membrane is much slower than a diffusion-limited rate. It is limited by a significant free energy barrier to membrane association, which can be estimated from the ratio of the reaction rate compared to the diffusion limited reaction velocity, where $\Delta G^{\ddagger} = -RT \ln(k_1/v) \approx 28$ kJ/mol at 298 K. This result represents the free-energy barrier for GLP-1 to associate with the lipid bilayer surface. It could arise from only a small fraction of peptide conformations being favorable to membrane association, changes in peptide solvation, and/or the requirement for phospholipids in the bilayer to adopt specific conformations to accommodate the adsorbed peptide. The conformational changes required for initial membrane affiliation by the peptide may be related to the small free energy difference $\Delta G = -1.7$ kJ mol^{-1} between W and S states determined above, where the W state is already significantly folded to affiliate with the membrane, so that a relatively small free energy difference is found in the transition to the strongly bound form.

5. DISCUSSION

The present results illustrate the utility of measuring peptide residence times and populations on supported lipid bilayers by single-molecule imaging as a means of determining kinetics of their membrane affiliation. With careful attention to detection criteria, absolute populations of membrane-associated peptides can be measured at very low concentrations in solution and on the membrane surface, typical of physiological conditions. Within the context of the reversible three-state, two-step model, the microscopic rates determined from the residence time analysis provide insight into dynamics controlling the membrane-bound population of peptide, the fraction that is intercalated, and rates of transfer between the membrane−solution interface and a folded state within the membrane interior.

While the proposed sequential two-step model is rational and fully consistent with the data, it is not a unique scheme that would account for the biexponential decay of the peptide residence times in the membrane. The two populations, W and S, could be independently bound forms of the peptide, each with its own binding and unbinding rate from solution. These two populations might arise, for example, from differences in folding of the two helical domains of GLP-1.[8] Validation of the correct model for these binding kinetics, either sequential 2-step or independent bound states, could be guided by structural changes in the peptide to test their influence on the observed rates. For example, Exendin-4, an effective agonist for the GLP-1 receptor commercially produced for treatment of diabetes shares 50% sequence homology with GLP-1, but exhibits greater helical structure in an aqueous solution.[9,10] The tendency of this peptide to adopt an α-helix conformation prior to membrane association may contribute to its efficacy by lowering of barriers to membrane affiliation and intercalation. Measuring the changes in membrane binding equilibria and residence times for Exendin-4 or similar drug candidate peptides could provide important insight not only into their

structure−activity relationships but also into the appropriate kinetic model for their membrane interactions.

A limitation of the present GLP-1 results is that the peptide binding to the DPPC lipid bilayer was measured at 22 °C, a temperature below the 42 °C gel-to-liquid-crystal phase transition of DPPC.[41] Fluid or ripple phase lipids behave more like natural membranes than the gel-phase DPPC,[42,43] and the effects of the lipid phase and composition on the kinetics of peptide insertion would be an important goal for future work. These experiments introduce a measurement challenge, namely diffusion of the bound peptide in the fluid membrane environment. Peptide diffusion in gel-phase DPPC is minimal, which eases the measurement of residence times of stationary fluorescent spots; diffusion of peptides in a fluid membrane, such as POPC, requires tracking of molecules over time in order to report residence times.[44−46] Lateral diffusion of peptides in a membrane could be readily quantified and may provide additional evidence to characterize peptide−membrane interactions, including resolving weakly and strongly bound states based on differences in their lateral mobility. Also, lipid charge can have significant effects on the interactions of peptides with bilayers.[47] Although GLP-1 has a net-zero charge at neutral pH, it includes several regularly spaced negatively charged carboxylate groups which could exhibit charge repulsion with negatively charged lipid membranes that include small amounts of phosphatidylserine, for example.[48] Finally, as was successfully demonstrated for single-stranded DNA diffusing at solid−liquid interfaces,[49] it may also be possible to measure resonance energy transfer between different fluorescent labels on the C- and N-termini of the GLP-1 peptide to discriminate between random coil and α-helix conformations of the peptide in the membrane. The time evolution of these states could be useful information to validate the model used to interpret the binding kinetics.

The development of the mathematical relationships between residence time histograms, surface-bound populations, and the microscopic rates of the three-state kinetic model should be broadly applicable to other areas of interfacial chemistry where an adsorbed molecule can transition to a more tightly bound state. The solutions to these differential equations are also relevant to wash-off experiments commonly used in sensor development, where a surface is first equilibrated against a given solution concentration and then subjected to a concentration step to zero. This step is usually accomplished by flushing the reacted surface with buffer, while the decay in the remaining surface-bound concentration of molecules is measured over time.

The boundary conditions of such an experiment are, first, that the surface is at equilibrium with the solution at time zero. In other words, the initial fractions of weekly and strongly associated species are given by their equilibrium values:

$$W(0) = \frac{k_4}{k_3 + k_4} \tag{10a}$$

$$S(0) = \frac{k_3}{k_3 + k_4} \tag{10b}$$

The second initial condition in the wash-off experiment is the same as for residence time histograms: no molecules revisit the surface after unbinding, or in other words, k_1 is zero. When these initial conditions are applied to the general solutions given in eqs S2−S6 in Supporting Information, the counterpart to eq 1 for the sum of the populations of molecules in the W and S states remaining after the beginning of a wash-off has the identical form as eq 1, a biexponential decay without offset:

$$R(t) = P_{1R}\, e^{-r_1 t} + P_{2R}\, e^{-r_2 t} \tag{11}$$

where r_1 and r_2 are given by eqs 3a and 3b, and P_{1R} and P_{2R} for the normalized function are given by

$$P_{1R} = \frac{k_2 - k_3 - k_4 + (r_1 - r_2)}{2(r_1 - r_2)} - \frac{k_2 k_3}{(r_1 - r_2)(k_3 + k_4)} \tag{12a}$$

$$P_{2R} = \frac{-k_2 + k_3 + k_4 + (r_1 - r_2)}{2(r_1 - r_2)} + \frac{k_2 k_3}{(r_1 - r_2)(k_3 + k_4)} \tag{12b}$$

It can be shown that the derivative of this counterpart expression is proportional to eq 1, and when both are normalized, the constant of proportionality is the effective desorption rate: the product of the microscopic rate constant, k_2, and the fraction of molecules in the W state at equilibrium:

$$-\frac{\partial}{\partial t} R(t) = r_1 P_{1R}\, e^{-r_1 t} + r_2 P_{2R}\, e^{-r_2 t} = \frac{k_2 k_4}{k_3 + k_4} H(t) \tag{13}$$

The derivative of an exponential is equal to the exponential times the derivative of the exponential argument, thus to convert the pre-exponential terms of the wash-off experiment to the equivalent histogram pre-exponentials, one need only scale the results by the corresponding rate constant and evaluate the measured rates and pre-exponential values according to eqs 5−7 above to determine the microscopic rate constants, k_2−k_4.

The single-molecule imaging experiment has several advantages over a typical wash-off experiment. One advantage is that single-molecule imaging can report densities of bound molecules on the surface, while typical wash-off experiments are carried out at surface densities much too large for imaging and counting single molecules. In addition, the high surface coverages used in wash-off experiments can lead to molecule−molecule interactions that influence and confound both binding equilibria and kinetics. More importantly, single-molecule residence time measurements can be carried out at equilibrium and thus do not require the concentration step of a wash-off experiment to measure unbinding kinetics. In practice, slow mass transfer through the unstirred boundary layer near the surface makes it difficult to quickly remove molecules from the solid/liquid interface, in order to prevent the rebinding of molecules liberated from the surface. Thus, the condition that k_1 is zero during the wash-off experiment may not be met, and the decay in population of molecules on the surface is confounded by rebinding from solution and the slow mass transfer of molecules away from the surface.

■ ASSOCIATED CONTENT

Supporting Information

Analysis of differential equations for single-molecule binding, mass spectrometry data for GLP-1 labeling, optimization of image processing for bridging photoblinking events, intensity distributions to determine false-negative probabilities, binding isotherms for control samples, a log−linear plot of a residence time histogram, residence time kinetics versus laser power to evaluate photobleaching, and comparison of kinetic results acquired with different microscopes and dye labels. This

dx.doi.org/10.1021/ja306074k | J. Am. Chem. Soc. 2012, 134, 19652−19660

material is available free of charge via the Internet at http://pubs.acs.org.

AUTHOR INFORMATION

Corresponding Author

harrisj@chem.utah.edu

Present Address

[§]Infectious Disease Research Institute, 1124 Columbia St., Suite 400, Seattle, WA 98104

Notes

The authors declare no competing financial interest.

ACKNOWLEDGMENTS

This research was supported in part by the National Science Foundation under Grant CHE-0957242.

REFERENCES

(1) Sargent, D. F.; Schwyzer, R. *Proc. Natl. Acad. Sci. U.S.A.* **1986**, *83*, 5774.
(2) Castanho, M. A. R. B.; Fernandes, M. X. *Eur. Biophys. J.* **2006**, *35*, 92.
(3) Langelaan, D. N.; Rainey, J. K. *Biochem. Cell Biol.* **2010**, *88*, 203.
(4) Grieve, D. J.; Cassidy, R. S.; Green, B. D. *Br. J. Pharmacol.* **2009**, *157*, 1340.
(5) Van Gaal, L. F.; Gutkin, S. W.; Nauck, M. A. *Eur. J. Endocrinol.* **2008**, *158*, 773.
(6) MacDonald, P. E.; El-kholy, W.; Riedel, M. J.; Salapatek, A. M. F.; Light, P. E.; Wheeler, M. B. *Diabetes* **2002**, *51*, S434.
(7) Wieprecht, T.; Apostolov, O.; Beyermann, M.; Seelig, J. *J. Mol. Biol.* **1999**, *294*, 785.
(8) Thornton, K.; Gorenstein, D. G. *Biochemistry* **1994**, *33*, 3532.
(9) Neidigh, J. W.; Fesinmeyer, R. M.; Prickett, K. S.; Andersen, N. H. *Biochemistry* **2001**, *40*, 13188.
(10) Andersen, N. H.; Brodsky, Y.; Neidigh, J. W.; Prickett, K. S. *Bioorg. Med. Chem.* **2002**, *10*, 79.
(11) Xiaoqing, C.; Danielle, K.; Søren, B.; Jens, J. L. *Magn. Reson. Chem.* **2001**, *39*, 477.
(12) Underwood, C. R.; Garibay, P.; Knudsen, L. B.; Hastrup, S.; Peters, G. H.; Rudolph, R.; Reedtz-Runge, S. *J. Biol. Chem.* **2010**, *285*, 723.
(13) Constantinescu, I.; Lafleur, M. *Biochim. Biophys. Acta* **2004**, *1667*, 26.
(14) Papo, N.; Shai, Y. *Biochemistry* **2003**, *42*, 458.
(15) Fox, C. B.; Wayment, J. R.; Myers, G. A.; Endicott, S. K.; Harris, J. M. *Anal. Chem.* **2009**, *81*, 5130.
(16) Tolman, R. C. *The Principles of Statistical Mechanics*; Oxford University Press: London, 1938.
(17) Evans, M. G.; Polanyi, M. *Trans. Faraday Soc.* **1935**, *31*, 875.
(18) Eyring, H. *J. Chem. Phys.* **1935**, *3*, 107.
(19) Day, R.; Daggett, V. *J. Mol. Biol.* **2007**, *366*, 677.
(20) Walder, R.; Kastantin, M.; Schwartz, D. K. *Analyst* **2012**, *137*, 2987.
(21) Lowry, T. M.; John, W. T. *J. Chem. Soc. Trans.* **1910**, *97*, 2634.
(22) Wei, J.; Prater, C. D. In *Advances in Catalysis*; Eley, D. D., Selwood, P. W., Weisz, P. B., Eds.; Academic Press: New York, NY, 1962; Vol. *13*, p 203.
(23) Capellos, C. *Kinetic systems: mathematical description of chemical kinetics in solution*; Wiley-Interscience: New York, 1972.
(24) Hansen, R. L. *Anal. Chem.* **1998**, *70*, 4247.
(25) Starr, T. E.; Thompson, N. L. *Biophys. J.* **2001**, *80*, 1575.
(26) Bard, A. J.; Faulkner, L. R. *Electrochemical Methods: Fundamentals and Applications*, 2nd ed.; Wiley: New York, 2001.
(27) Charitat, T.; Bellet-Amalric, E.; Fragneto, G.; Graner, F. *Eur. Phys. J. B* **1999**, *8*, 583.
(28) Starr, T. E.; Thompson, N. L. *Langmuir* **2000**, *16*, 10301.
(29) Tamm, L. K.; McConnell, H. M. *Biophys. J.* **1985**, *47*, 105.
(30) Wayment, J. R.; Harris, J. M. *Anal. Chem.* **2008**, *81*, 336.
(31) Peterson, E. M.; Harris, J. M. *Anal. Chem.* **2009**, *82*, 189.
(32) Ambrose, W. P.; Goodwin, P. M.; Martin, J. C.; Keller, R. A. *Phys. Rev. Lett.* **1994**, *72*, 160.
(33) Lu, H. P.; Xie, X. S. *Nature* **1997**, *385*, 143.
(34) Yip, W.-T.; Hu, D.; Yu, J.; Bout, D. A. V.; Barbara, P. F. *J. Phys. Chem. A* **1998**, *102*, 7564.
(35) Gensch, T.; Böhmer, M.; Aramendía, P. F. *J. Phys. Chem. A* **2005**, *109*, 6652.
(36) Gao, F.; Mei, E.; Lim, M.; Hochstrasser, R. M. *J. Am. Chem. Soc.* **2006**, *128*, 4814.
(37) Hanley, D. C.; Harris, J. M. *Anal. Chem.* **2001**, *73*, 5030.
(38) Sun, S.; Luo, N.; Ornstein, R. L.; Rein, R. *Biophys. J.* **1992**, *62*, 104.
(39) Zagrovic, B.; Jayachandran, G.; Millett, I. S.; Doniach, S.; Pande, V. S. *J. Mol. Biol.* **2005**, *353*, 232.
(40) Rice, S. A. In *Comprehensive Chemical Kinetics*; Bramford, C. H., Tipper, C. F. H., Compton, R. G., Eds.; Elsevier: Amsterdam, 1985; Vol. *25*.
(41) Koynova, R.; Caffrey, M. *Biochim. Biophys. Acta* **1998**, *1376*, 91.
(42) Pott, T.; Dufourcq, J.; Dufourc, E. J. *Eur. Biophys. J.* **1996**, *25*, 55.
(43) Sekharam, K. M.; Bradrick, T. D.; Georghiou, S. *Biochim. Biophys. Acta* **1991**, *1063*, 171.
(44) Ishihara, A.; Jacobson, K. *Biophys. J.* **1993**, *65*, 1754.
(45) Simson, R.; Sheets, E. D.; Jacobson, K. *Biophys. J.* **1995**, *69*, 989.
(46) Saxton, M. J.; Jacobson, K. *Annu. Rev. Biophys. Biomol. Struct.* **1997**, *26*, 373.
(47) Ahyayauch, H.; Raab, M.; Busto, J. V.; Andraka, N.; Arrondo, J.-L. R.; Masserini, M.; Tvaroska, I.; Goñi, F. M. *Biophys. J.* **2012**, *103*, 453.
(48) Bong, D. T.; Janshoff, A.; Steinem, C.; Ghadiri, M. R. *Biophys. J.* **2000**, *78*, 839.
(49) Kastantin, M.; Schwartz, D. K. *ACS Nano* **2011**, *5*, 9861.